Medicine in Novel Technology and Devices 11 (2021) 100090

Contents lists available at ScienceDirect

Medicine in Novel Technology and Devices

journal homepage: www.journals.elsevier.com/medicine-in-novel-technology-and-devices/

Full Length Article

Spinal deformity measurement using a low-density flexible array ultrasound transducer: A feasibility study with phantoms

Queenie Tsung Kwan Shea, Yan To Ling, Timothy Tin-Yan Lee, Yong Ping Zheng *

Department of Biomedical Engineering, The Hong Kong Polytechnic University, Hong Kong SAR, China

ARTICLE INFO

Keywords:
Flexible ultrasound array
Low-density array
Spinal deformity
3D ultrasound

ABSTRACT

Spinal deformities assessment using 3D ultrasound scanning has limitations in fitting onto different back surface contour as well as fitting within the gaps between subject and their spinal brace during bracing assessments. The study proposed a flexible array ultrasound transducer to overcome these limitations.

The results demonstrated the feasibility of spinal deformity assessments with a flexible ultrasound array when arranged in four shapes, namely Linear, Concave, Convex, and S-shaped. For comparisons of imaging performance on spinous process using the four shapes, Convex and S-shaped transducer showed a depth dependence and lateral location dependence of the lateral intensity distribution of spinous process, respectively. S-shaped transducer had the least accurate prediction of the location of spinous process, with measurement error of 4.8 ± 3.2 mm, it also showed poorer prediction on spinal curvature measurements. This is suggested to be due to the asymmetrical distortion to the spinous process due to the lateral location dependence of the image. However, the coronal curve prediction of spine phantom performed well with R-squared values of >0.97 in all transducer shapes.

The results of this study paved the way for further investigation on the improvement of image quality and measurement accuracy under different shapes for the flexible array, mechanism of dynamic shape change during the scanning to fit different body contour, as well as extension from 1D to 2D flexible array.

1. Introduction

Scoliosis is defined as a medical condition in which a person's spine has a curve larger than 10° in the coronal plane. Scoliosis is commonly associated with back pain [1], and lung [2] or heart problems [3]. Adolescent idiopathic scoliosis (AIS), the most common form of scoliosis, affects 1–3% of the children at 10–16 years [4]. To provide diagnosis for this disease, the gold standard is to measure the Cobb angle of patient's spine using standing X-ray assessment on the coronal plane [5]. Once scoliosis is diagnosed, regular X-ray assessments on patients are required to monitor curvature progression and treatment outcome. However, frequent assessment using X-ray has radiation hazards and may increase risk of cancer [6]. The EOS (EOS imaging, Paris, France) provided a low-dose biplanar radiography for scoliosis assessment, but it still utilizes ionizing radiation and does not provide direct 3D information [7]. In addition, the cost of EOS is much higher than ordinary X-ray imaging machines, thus not affordable in most clinics.

Ultrasound imaging combined with 3D spatial sensor has recently been demonstrated to give reliable measurement about spinal deformity angles [7–15]. This imaging method does not involve the use of ionizing radiation for scoliosis assessments comparing to X-ray examination. As the ultrasound images are reconstructed in 3D space, it could also provide deformity information of the spine in 3D, further providing diagnostic information such as deformity angle in sagittal plane [16]. To perform this imaging, operators need to move the ultrasound probe vertically up along the subject's back. The bony features, such as spinous processes, are then identified from the ultrasound images for spinal deformity assessment. However, it was reported that a large amount of gel is needed to fill the gaps between the body surface and the conventional rigid ultrasound transducer, where image qualitiy are often affected when air gaps are present between transdcuer and the body surface. This is because the subject's back has complicated contour, in both sagittal and transverse plane of the human body. The situation can be even worse when the subject has severe spinal deformity, such as in the case of severe scoliosis. Moreover, it is currently difficult to perform imaging in subject when they are wearing spinal brace [17]. As spinal brace is designed to maintain pressure on the body surface of the subject, any opening on the brace could affect this pressure. Supporting the

* Corresponding author.
E-mail addresses: queenie.tk.shea@connect.polyu.hk (Q.T.K. Shea), jane.yt.ling@connect.polyu.hk (Y.T. Ling), timothy.lee@connect.polyu.hk (T.T.-Y. Lee), yongping.zheng@polyu.edu.hk (Y.P. Zheng).

https://doi.org/10.1016/j.medntd.2021.100090
Received 31 October 2020; Received in revised form 21 July 2021; Accepted 23 July 2021

subject with brace mimicking frames, such as in the study conducted by Lou et al. [17], might not provide very accurate assessment on the actual brace.

To overcome these limitations, we proposed a method to use flexible array ultrasound transducer, which can fit with the subject's back during ultrasound scanning. This may facilitate a smooth scanning along the subject's back. Once the feasibility of using 1D flexible array is demonstrated, 2D flexible array can be further developed, which will potentially provide a dynamic ultrasound imaging method of the spine where no movement of the probe is needed. More importantly, it can also be used when the brace is worn normally by subjects, which helps to provide accurate examination for the brace fitting and the performance of brace treatment.

In this study, we focused on the feasibility of measuring spinal deformity using a 1D flexible array configured into different shapes. Evaluation on ultrasound images quality, spinous process 3D location accuracies as well as spinal deformity angle measurements were conducted using plastic spine phantoms with different spinal deformities. It has been previously reported that spinous process angle (SPA) in the coronal plane had a high reliability and accuracy for curvature measurement of scoliosis, in 3D ultrasound [7], in coronal plane X-ray [18] and in sagittal plane X-ray [19]. Therefore, we chose to use spinous process as the reference landmark for measurement of spinal deformity in both coronal and sagittal planes in this study.

2. Materials and methods

2.1. 1 design and control of flexible array ultrasound transducer

The transducer array used in this experiment was a custom-made 1D flexible array transducer (Guangzhou Doppler Electronics Co., Ltd, Guangzhou, China). The array consisted of 128 piezoelectric elements with pitch size of 1.1 mm. The center frequency of the transducer was 5 MHz, with a −6 dB relative bandwidth of 65 %. Each transducer element was 1 mm in width and 12 mm in length. The array was designed to allow flexible bending on the lateral dimension but not on the elevation dimension. Fig. 1 shows the bending flexibility of the transducer array.

To demonstrate the performances of the flexible array under different shapes, the array was fixed into four different shapes, namely Linear, Concave, Convex and S-shaped, using thermal deformable plastic plates (Orfit NS, Orfit Industries, Wijnegem, Belgium). The Linear transducer array had a straight arrangement of transducer elements. Both Concave and Convex transducer arrays had a radius of curvature of 100 mm and S-shaped transducer array had two curves with radii of around 50 mm. These shapes were chosen to mimic the shape of different body surfaces and possible deformation of the flexible array during imaging.

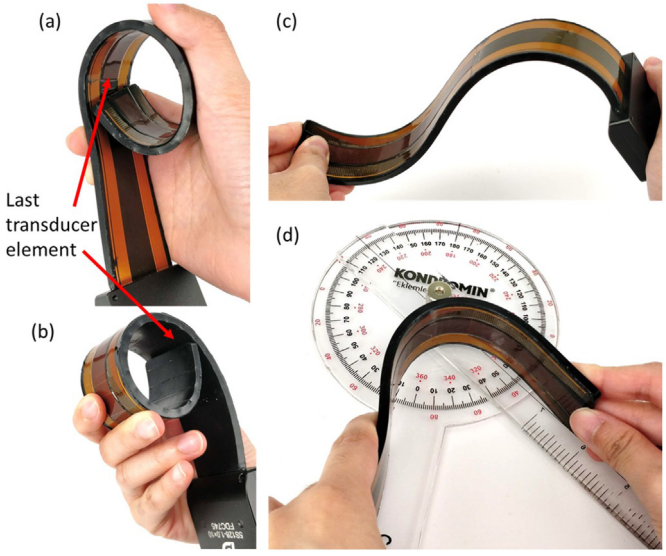

Fig. 1. Pictures of the flexible ultrasonic transducer array prototype. (a) and (b) demonstrating the bending ability of the transducer array, which could have full 360° angular coverage in both inward and outward bending. (c) demonstrating the bending ability of the array in complex geometry; (d) showing the minimum radius of curvature when bending the is approximately 30 mm.

The flexible array was first placed on a solid surface of a desired shape, a thermal deformable plastic plate which was preheated in a 70 °C water bath was molded to the back of the array and cooled down to room temperature. The four shapes of the flexible array were recorded using a 3D digitizer (MicroScribe-3DX, Solution Technologies, Inc., USA), by placing the 3D digitizer measurement tip at the center of each ultrasound piezoelectric element. The information was then used for ultrasound transmission beam forming and image reconstruction.

2.2. Image formation

Control of ultrasound transmission and acquisition was performed by a 128-channel ultrasound system (Vantage 128™, Verasonics, Inc., USA). The information of transducer shape was inputted into the system for control of transmission and acquisition. Image formation method chosen in this study was classical dynamic focusing transmission method. Dynamic focusing at 3 depths of 62 mm, 92 mm, and 123 mm along the 128 transmission lines defined in the image space was performed in each frame of capture.

To test the precision of spinous process measurement on images generated by the four array shapes used, the dimensions of the spinous process on the ultrasound images were examined. Ultrasound images were generated by placing the transducer array above extracted spinal vertebra phantom (Highly Flexible Spine Model, 3B Scientific, Hamburg, Germany) at T2 level as shown in Fig. 2. In separate trials, the spinous process was put at ten different locations in the frame, at 25 mm or 50 mm depth, and at each depth the lateral position of the spinous process was in the lateral center of the frame, and 20 mm and 40 mm to the left and right from the lateral center of the frame.

The locations of the spinous process in the images were manually identified. Rectangular regions of interest (ROI) with lateral width of 55 mm and axial length of 11.5 mm to include the full spinous process tip in all images were selected at the location of spinous process tip in each image. The lateral intensity distribution of the spinous process was taken by summing the intensity at the axial direction in the ROI. The lateral width of the spinous process in the image was measured at −6 dB intensity cut-off of the lateral intensity distribution. Pairwise comparisons were performed to compare the lateral intensity distribution between different depths, center or non-center, distance away from center, and

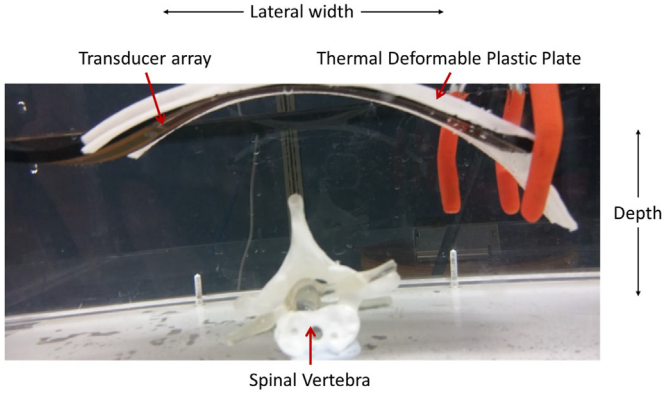

Fig. 2. Picture of the experimental setup for acquiring ultrasound images from a spine phantom with the flexible transducer submerged in a water tank, bubbles on the surface of the transducer are carefully removed before imaging.

left or right of the image of different transducer shapes. One-way ANOVA was performed to compare the differences between different transducer shapes in all locations within the frame. $p < 0.05$ was regarded as significantly different.

2.3. Measurements of 3D coordinates of spinous processes

Four plastic spine phantom models (Highly Flexible Spine Model, 3B Scientific, Hamburg, Germany) were used in this experiment to perform 3D ultrasound imaging. The phantoms were fixed into four different curvatures commonly found in patients with scoliosis. Fig. 3 shows the deformity of the phantoms along coronal plane observed from posterior view. Fig. 3a shows the shape of spine phantom 1, with a single right thoracic curve. Fig. 3b shows the shape of spine phantom 2, which was relatively straight but with mild double curves at thoracic and lumbar regions. Fig. 3c shows the shape of spine phantom 3, with a major left thoracic curve. Fig. 3d shows the shape of spine phantom 4, with lordosis on sagittal plane and a small S-shaped curve on coronal plane.

Each phantom was submerged into a water tank with the posterior side facing upward. The transducer array facing down was fixed onto a linear stepper motor (SH–120S, Shenzhen Shenhuaya Technology Co. Ltd., Shenzhen, Guangdong, China), which was controlled by stepper motor driver (DM542, Leadshine Technology Co. Ltd., Shenzhen, Guangdong, China). The ultrasound image plane was carefully aligned perpendicularly to the direction of the motor movement manually, as illustrated in Fig. 4. The transducer was in contact with the water to ensure acoustic coupling to the spine phantom.

Scanning was performed from the lowest lumbar vertebrae (L5) to the highest thoracic vertebrae (T1). The motor was synchronized with the image capturing of the ultrasound system to ensure the timing of each image captured between each step of motor movement, to avoid motion artifacts.

The captured ultrasound images with the corresponding 3D location and orientation were imported into a customized 3D ultrasound image reconstruction program to form a 3D volume data. The spinous process was manually selected in a custom-made 3D visualization program shown in Fig. 5 for displaying 3D ultrasound scanning on spine. The location of the tip of the spinous processes was selected manually in the 3D visualization program at the B-mode image plane by finding the B-mode image in the lowest position of the 3D volume where the spinous process was still visible. A location landmark was placed at the tip of the spinous process of the selected B-mode image to record its 3D location.

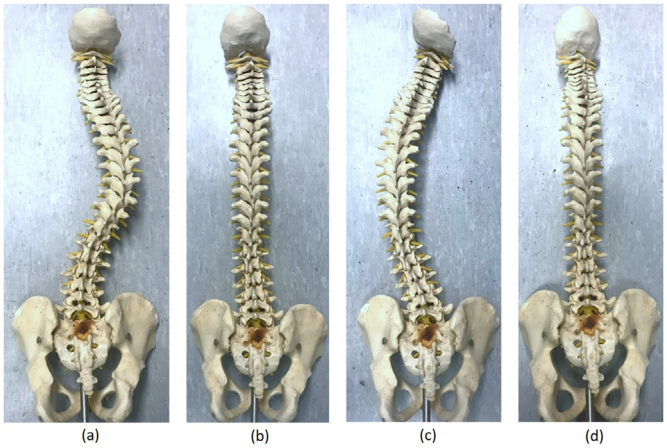

Fig. 3. Pictures of the four spine phantoms used. (a) spine phantom 1, with a thoracic curve bending to the right, (b) spine phantom 2, which was relatively straight but with small double curves at thoracic and lumbar regions, (c) spine phantom 3, with a major thoracic curve bending to the left, (d) spine phantom 4, with hyperlordosis on sagittal plane and a small S-shaped curve on coronal plane.

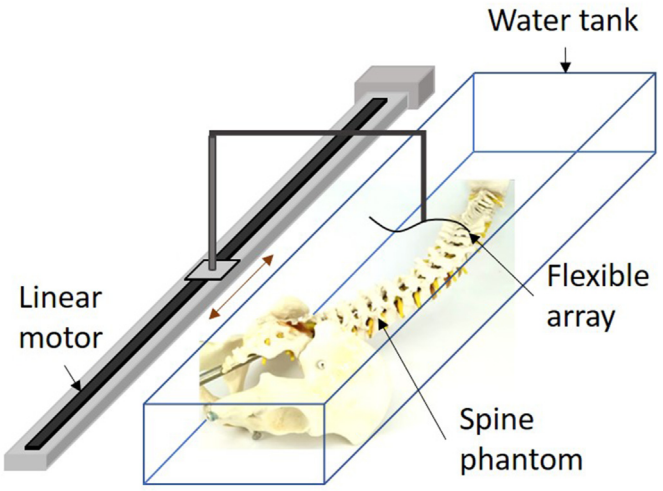

Fig. 4. Illustration of the setup of linear motor and the flexible transducer array to preform scanning on the spine phantom in a water tank. Water level was above or at the transducer array to ensure acoustic coupling to the spine phantom.

The projection images of the 3D volume at the coronal and sagittal planes were used to confirm the location of the spinous process was selected correctly on the B-mode image. These projection images were generated with a non-planar reslice defined by the location of all the spinous processes selected, where the method for generating projection image was the same as described by a previous study [7]. Fig. 5 shows the software interface used to preform measurements of 3D locations of spinous process.

A 3D digitizer (MicroScribe-3DX, Solution Technologies, Inc., USA), was used to measure the 3D coordinates of the spinous processes on the same spine phantoms for comparisons. The location accuracy of the 3D digitizer is 0.23 mm. The coordinates of the spinous processes were measured by placing the measurement tip of the 3D digitizer onto the posterior end of the spinous process, from L5 to T1. The spine phantoms were arranged in prone position during the measurement, and the reference frame was adjusted with reference to the floor so that the x-y plane is at the same plane as the coronal plane of the spine.

2.4. Comparing 3D coordinates of spinous processes

As the 3D coordinates of the spinous process could be measured in a slightly different reference frame during scanning with the array transducer and measurement with the 3D digitizer, the reference frames of these coordinates had to be corrected before comparing among different setups. Therefore, the 3D reference frames of coordinates measured by the ultrasound transducer arrays were corrected based on the coordinates measured by 3D digitizer on the same spine phantom. The correction was achieved by finding the minimum distance between the two sets of coordinates under translation (shifting) and rotation with respect to x, y, and z axes. First, shifting along the 3 axes were performed one by one with the defined shifting precision, a shifting value which gave minimum distance between both sets of spinous process coordinates was chosen and corrected. After shifting in all axes were corrected, rotation around the 3 axes were performed one by one to find the optimal rotational angle in all axes. The precisions defined here were 0.01 mm in shifting and 0.01 rad in rotation. The process was repeated until the resulting mean distance between spinous processes did not change more than 0.1 mm compare to the previous step. Fig. 6 illustrates the method of correcting the reference frame.

After correcting the reference frame, the distances between spinous process locations measured by the 3D ultrasound image were compared with their corresponding locations measured by the 3D digitizer.

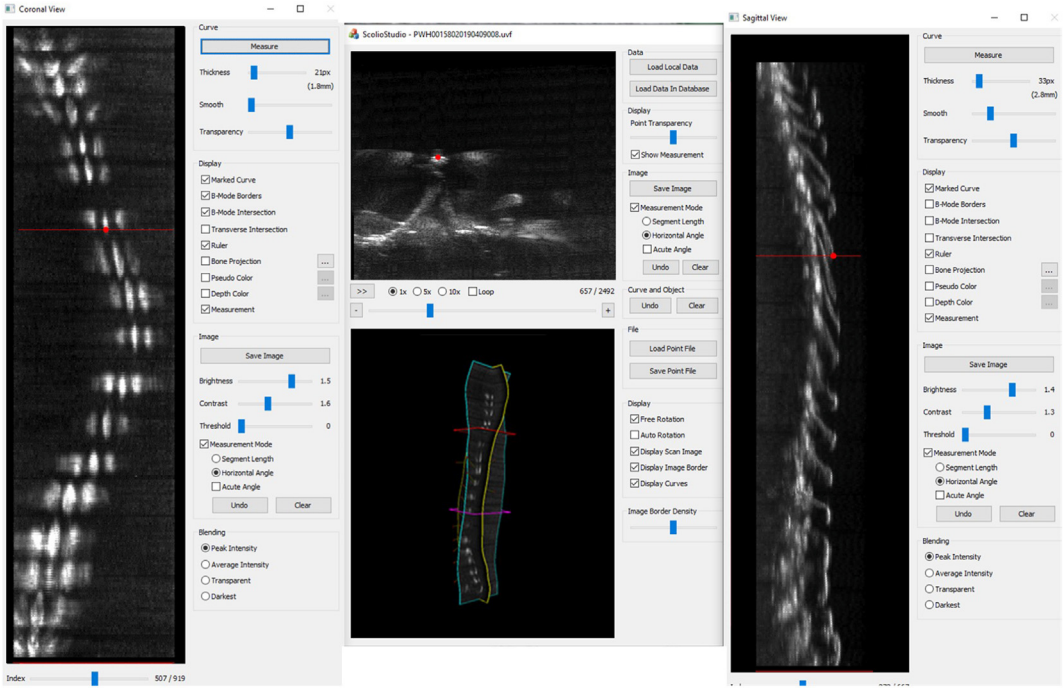

Fig. 5. Figures showing the user interface of the 3D visualization software. The left and right windows show the coronal and sagittal view projection image respectively. The top part of the center window shows the B-mode image at the selected level (indicated by red line in the other windows) in the 3D space. The bottom part of center window shows the 3D volume and location of the non-planar reslice of coronal and sagittal plane projection images, yellow line as the sagittal plane projection image reslice, blue line as the coronal plane projection image reslice. The upper red plane is the B-mode plane as shown on center top window. The location of the spinous process tip was identified at the B-mode image at the lowest position of the 3D volume (indicated by red dot) of the spinal vertebrae selected from the coronal and sagittal plane projection images. The 3D coordinates of the landmarks were extracted from the program for further processing.

Distances were calculated by the root-mean-square of the Euclidean distance in x, y, and z axes, which was the straight-line absolute distance between the tips of the two coordinates of corresponding spinous processes. The mean distance of all spinous processes and its standard deviation were calculated for comparisons among different shapes of array. Two-way analysis of variance (ANOVA) was performed to compare the distance between 3D digitizer measurements and 3D Ultrasound for different transducer shapes and in different phantoms. $p < 0.05$ was regarded as significantly different.

2.5. Spinous process angle measurements

To assess the deformity of the spine, an ultrasound volume projection imaging of spinous processes (VPI-SP) method was previously reported [7]. This method proposed that the deformity of spine in coronal plane could be assessed by the projection curve of the spinous processes. It was demonstrated that the measurement using VPI-SP method could have a close correlation with the coronal plane Cobb's angle measurements based on X-ray.

In this study, a similar method was used on the curve projected from the spinous process coordinates. The spinous processes coordinated at the coronal and sagittal plane were extracted. Using the semi-automatic curve detection method proposed in Ref. [20], the coordinates were fitted with 6th order polynomial curve, and the angle of normal at two adjacent inflection points were obtained for spinal curvature assessments. As spine phantoms with spinal deformity of single-curved or double-curved were included, a maximum of three inflection points were used in the calculations. Hence, only maximum of 2 spinal deformity angles was documented for each curve.

Linear regression was performed for the deformity angles measured by the 3D digitizer and the 3D ultrasound imaging based on flexible array transducer to investigate the performance of the proposed method. Pearson coefficients were calculated to describe the correlation of the angle measured by the transducer and the 3D digitizer.

3. Results

3.1. Spinous process measurement accuracy on 2D ultrasound image

Fig. 7 shows B-mode ultrasound images generated on the T2 vertebrae using the four different transducer shapes. The B-mode images were observed for qualitative comparisons. It was observed that the B-mode image obtained by the linearly configured transducer shows a clear contour of the spinal vertebrae, spinous process tip, both lamina and relatively weaker contour of the transverse process (Fig. 7a). For Convex, Concave and S-shaped transducers (Fig. 7b, c, Fig. 7d), the shape of spinous process and lamina could be observed with weaker contour than Convex transducer. Similar image features were observed in vertebra at other levels.

Quantitative comparisons of the images were conducted at the ROI of spinous process, as shown in Fig. 8. The widths of the spinous process tips in the image were measured with loss of −6 dB intensity from maximum in the lateral dimension within the ROI in Fig. 9. Fig. 10 shows the mean measured width of the spinous process measured at 10 different locations with the four different shapes of transducers, which are 4.0 ± 0.8 mm, 10.6 ± 4.9 mm, 12.0 ± 6.5 mm, and 8.5 ± 3.3 mm for Linear, Convex, Concave, and S-shaped transducer, respectively. Significant differences were found between Linear and Convex ($p < 0.05$) and between Linear and Concave shape transducers ($p < 0.05$).

Comparisons of location dependence of lateral intensity distributions of the four transducer shapes only showed significant differences for Convex shapes on depth and S-shape on left or right of the image. Convex has significantly wider lateral distribution in deeper 50 mm depth of 14.9 ± 2.5 mm than 25 mm depth of 6.4 ± 2.2 mm. S-shaped has significantly wider lateral distribution in concave lateral side of 10.4 ± 2.5 mm than convex lateral side of 5.4 ± 1.9 mm. None of the four

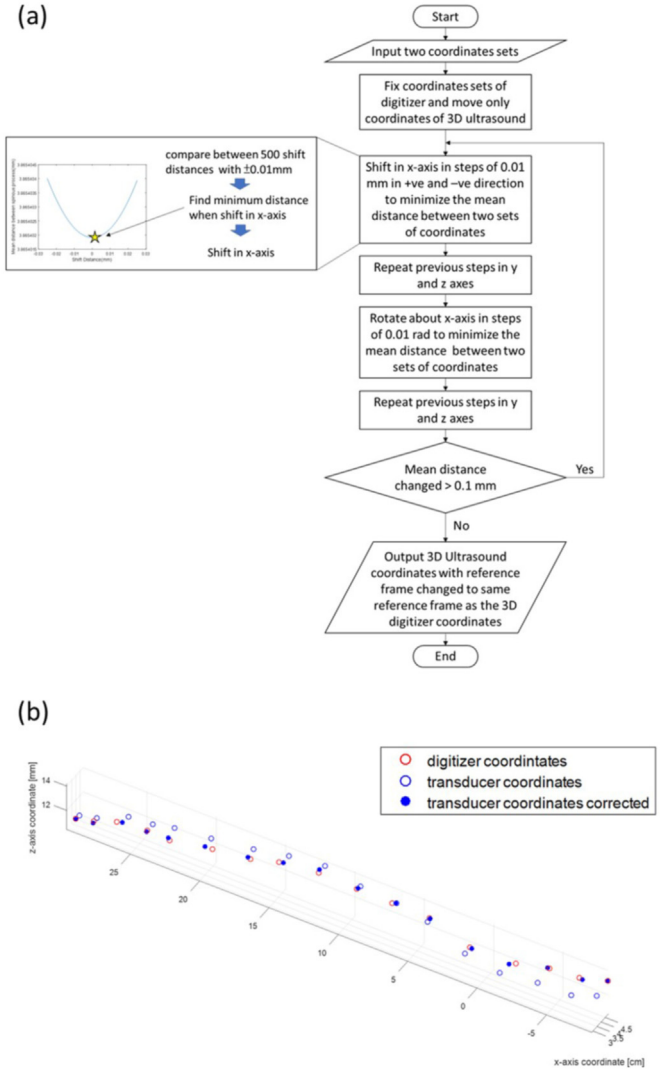

Fig. 6. (a) Diagram illustrating the procedures of correcting the reference frame of two sets of coordinates iteratively. The coordinates are translated and rotated at steps of 0.01 mm and 0.01 rad in positive and negative directions of 500 steps in 3 axes. The best translation distance and rotation angle are chosen by comparing the absolute distance between all points in the two sets of coordinates. The process of correction in translation and rotation were repeated until the change in mean distance is less than 0.1 mm. The corrected reference frame of the coordinates measured by 3D ultrasound images were outputted. (b) Coordinates of spinous processes measured by 3D digitizer and transducer before and after reference frame correction. Red circles represent the location of coordinates measured by 3D digitizer. Blue circles represent the location of coordinates measured by flexible array; before correction (no fill) and after correction (solid fill).

shapes has shown significant differences for different distances away from the center on the lateral direction. The spatial dependence of lateral distribution of spinous process in S-shapes and Convex transducer suggested that the accuracy on measuring location of spinous process would be affected by the location of spinous process on the frame, where Convex would have less accurate measurement at deeper region and S-shape would have less accurate measurement at the concave side.

3.2. Measurement accuracy of spinous process 3D location

The location measurement accuracy of the spinous process coordinates was evaluated by comparing the mean distance between coordinates measured by the 3D digitizer and the proposed 3D ultrasound

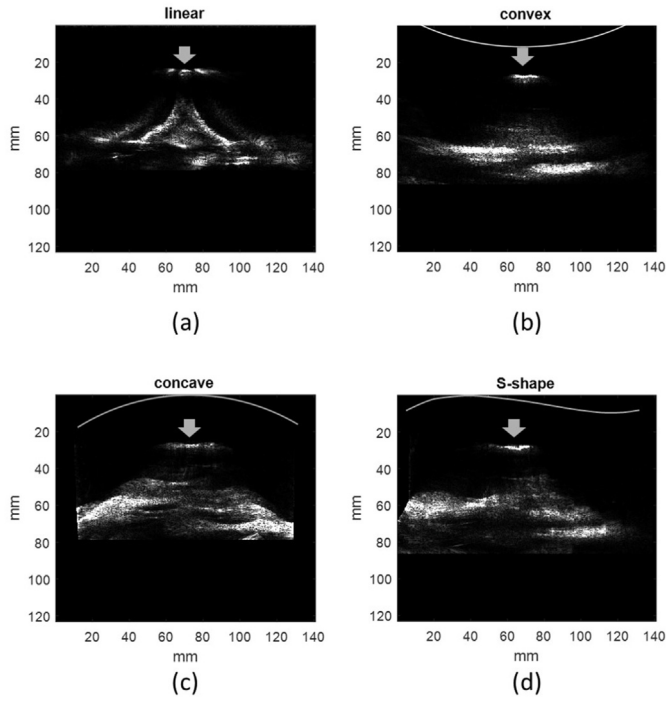

Fig. 7. Ultrasound images generated by the focused beam forming method using the flexible array arranged in (a) Linear, (b) Convex, (c) Concave and (d) S-shaped. The arrows indicate the location of the spinous process tip at each image.

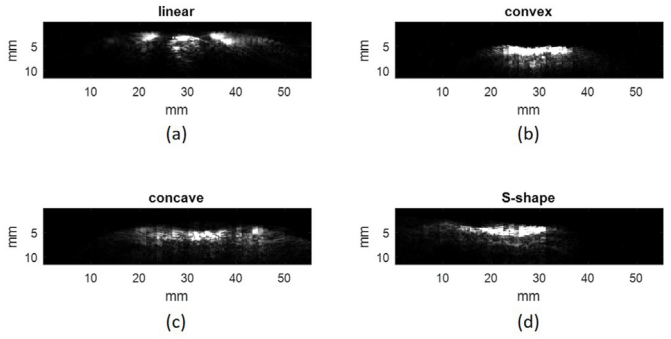

Fig. 8. The enlarged portions of images which shows the selected ROI of the spinous process formed by the Linear (a), Convex (b), Concave (c), and S-shaped (d) transducer array, respectively on the T2 level vertebrae phantom when spinous process is located at center of frame laterally and at 25 mm depth.

imaging method, at 17 levels of spinal vertebrae from T1 to L5, with the assumption that the 3D digitizer had accurate measurement for the spinous process tip location. No significant differences were found between different phantoms. However, S-shaped transducer had significantly larger mean distance of 4.8 ± 3.2 mm than the three other shapes; Linear 2.7 ± 1.5 mm, Convex 3.3 ± 1.9 mm, Concave 3.2 ± 3.0 mm, as shown in Fig. 11.

3.3. Spinal deformity angle on coronal and sagittal plane

A linear regression between the angles measured with the transducer arrays and the 3D digitizer was shown in Fig. 12 for the coronal plane and Fig. 13 for the sagittal plane. For the coronal plane, all regressions showed high correlation (R-squared value > 0.9). However, it could be observed that the S-shaped transducer tended to have overestimation of deformity angle, where the slope of regression was 1.15 with y-intercept

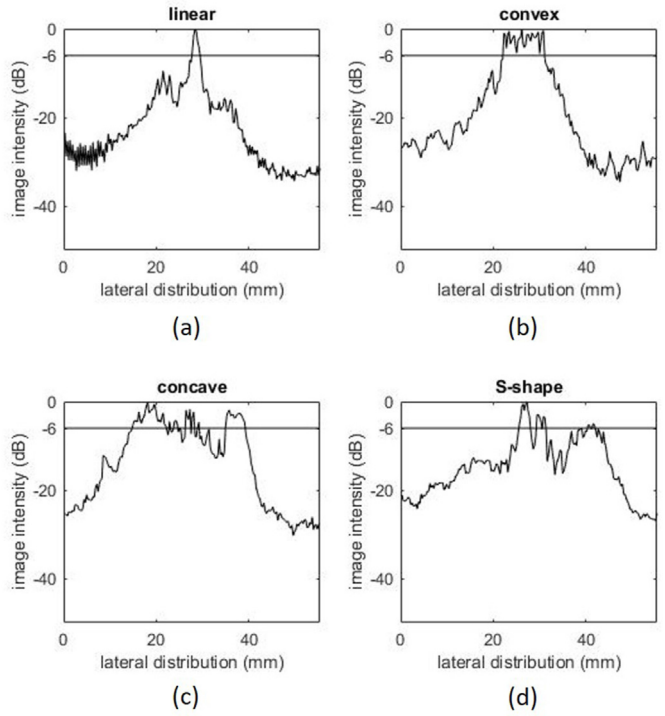

Fig. 9. The intensity distribution at the spinous process of T2 vertebrae from the area shown in Fig. 8. The distribution at the lateral axes where the intensity was summed in axial direction.

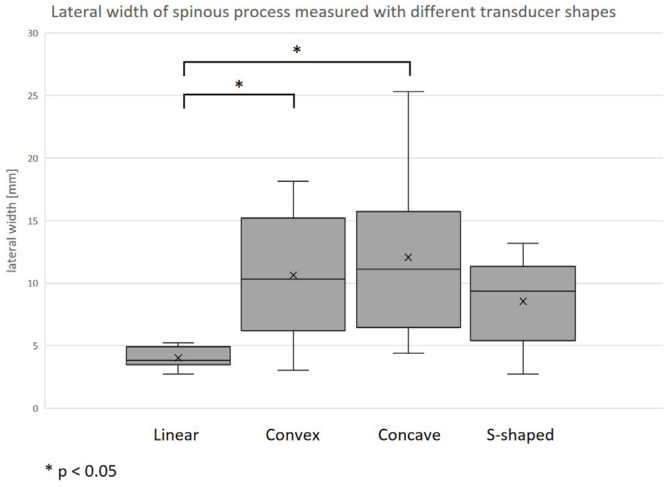

Fig. 10. The distribution of lateral width of the spinous process in the ultrasound B-mode images generated by Linear, Convex, Concave, and S-shaped transducer at 10 different locations within the frame (25 mm depth: center, 20 mm to left, 40 mm to left, 20 mm to right, 40 mm to right; 50 mm depth: center, 20 mm to left, 40 mm to left, 20 mm to right, 40 mm to right).

at 3.9°. For the sagittal plane, the correlation R-squared values were smaller than those measured on the coronal plane, which could be due to smaller range of angle in the sagittal plane (Fig. 13). The R-squared values were 0.88, 0.84, 0.60, and 0.66 for Linear, Convex, Concave, and S-shaped, respectively.

4. Discussion

This study compared the quality of 3D ultrasound images formed for spinous process phantoms using a flexible array ultrasound transducer

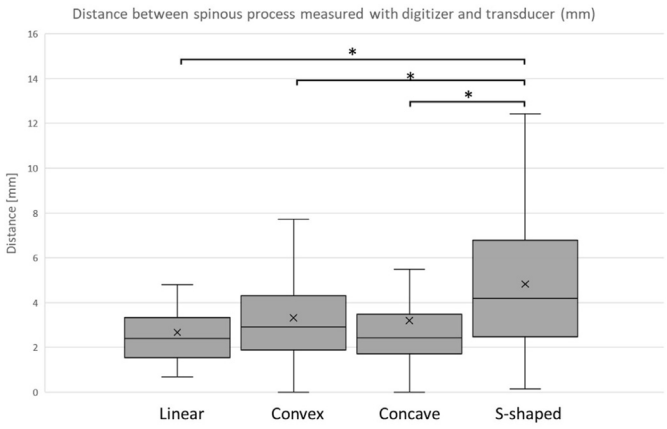

Fig. 11. Distance between spinous process measured with digitizer and transducer of Linear transducer, Convex transducer, Concave transducer, S-shaped transducer.

configured in Linear, Concave, Convex, and S-shaped arrangement with a dynamic focusing transmission method. Accuracies in measuring the location of the spinous processes, and spinal deformity angle were also compared between the four shapes. Linear transducer shape, as a reference shape to conventional linear transducer array, produced the best imaging quality as well as accuracy in measurements. This is because the uniform direction of the transducer elements in this arrangement allows more accurate prediction on the direction of reflected ultrasound wave. Meanwhile, the feasibility of using other shapes to obtain images from spine phantoms for spine deformity measurement was also demonstrated.

The lateral distribution of spinous process intensity of different transducer shapes provided insights on the accuracy of spinous process location measurements. Where Concave and Convex transducers had significantly wider intensity distribution compared to Linear transducer, the convex and concave side dependence of the lateral intensity distribution of the S-shaped transducer and the depth dependence of convex transducer had introduced inaccuracy of position measurements of the spinous process when the spinous process was at different locations within the frame.

It was noted that the accuracy in location and spinal deformity angle measurement after 3D reconstruction were the lowest in S-shaped transducer, while only Concave and Convex transducer shapes showed significantly wider lateral distribution of spinous process. However, this could be explained by a possible low accuracy introduced by the asymmetrical shape of S-shaped transducer. Due to the wider lateral intensity distribution in the concave side of the S-shaped transducer, the spinous process echo in the ultrasound image could be deformed towards the concave side of the transducer, causing a translation error of the spinous process location in the image.

For the deformity angle measurement, the S-shaped transducer also had the least accurate perdition of the coronal curve. This result shows that in order to improve accuracy for spinal deformity angle measurement, the focus should not be only on narrowing the intensity distribution of the reflector (i.e. spinous process) in the ultrasound image. The measurement accuracy of the deformity angle would highly depend on the measurement accuracy of the spinous process location, which could be reduced if an asymmetrical transducer shape such as the S-shaped transducer was involved.

Concave transducer on the other hand, had the widest lateral distribution of spinous process echo in the image, which was the major factor contributing to inaccuracy in prediction of the spinal deformity angle. Where all the transducer elements were facing towards the center of the frame, ultrasound echoes reflected from the center of the frame to different directions can be received strongly by most of the transducer elements on the Concave transducer. This had caused the lateral

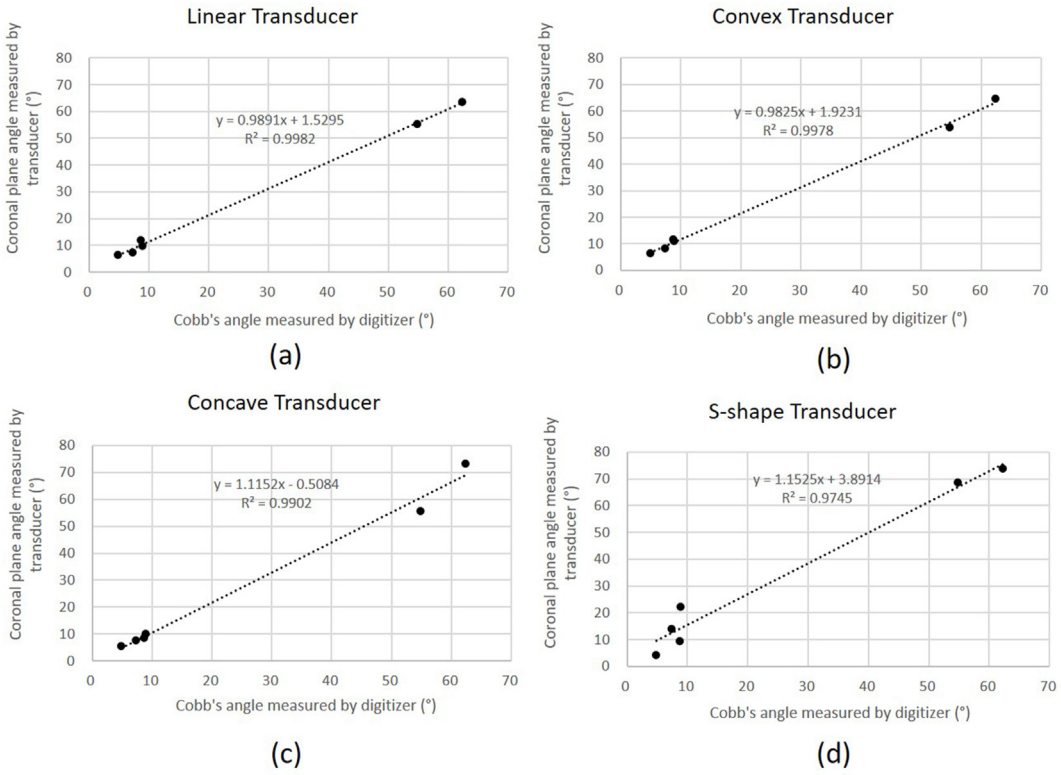

Fig. 12. Regression of deformity angle in coronal plane measured by the ultrasound transducer (vertical axis) and the 3D digitizer (horizontal axis). (a) Linear transducer, (b) Convex transducer, (c) Concave transducer, (d) S-shaped transducer.

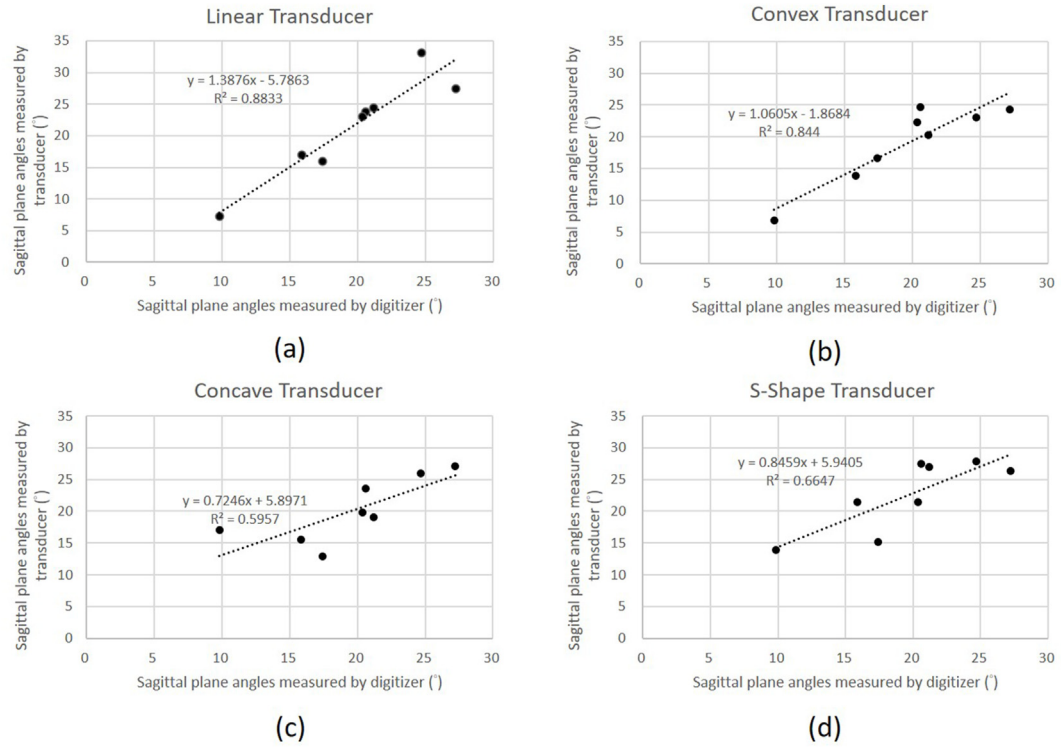

Fig. 13. Regression of deformity angles in sagittal plane measured by the ultrasound transducer (vertical axis) and the 3D digitizer (horizontal axis). (a) Linear transducer, (b) Convex transducer, (c) Concave transducer, (d) S-shaped transducer.

distribution of the spinous process to be wider in this shape. Therefore, future reconstruction methods should also consider the factors of directivity of elements in the Concave shape arrangement.

A limitation of this study was the assumption that the 3D digitizer was able to give accurate measurements. However, as provided by the manufacturer, the 3D digitizer has position accuracy of 0.23 mm. The

accuracy of 3D digitizer will contribute less than 10 % error to the measurements of relative location of spinous process measured by 3D digitizer and transducer array.

The present study is an important step towards the aim of scanning the subject's back using a flexible transducer to fit different contour along the back, by testing 4 different shape configurations for the 1D flexible transducer. It has been demonstrated that image of spine phantom could be successfully formed with Linear, Concave, Convex, as well as S-shaped transducers. The flexible array used in this study had a pitch of 1.1 mm, and width of each element of 1 mm, which is far from ideal for 5 MHz array. Therefore, further efforts are required to improve the flexible array with more optimized pitch and number of elements to achieve better image quality, which may improve the performance for all the 4 shapes tested. Future studies with improved image quality and increased density of elements will be compared with conventional ultrasound transducer array for the image quality and accuracy of spinous process location measurements.

Further in vivo investigation on human subject is also needed while allowing the transducer to bend dynamically. Methods for detecting transducer curvature dynamically such as topographic surface sensing technology using PVDF film [21] should be tested. The beam forming method has already been readied for any shape configuration, and the main technical challenge is the accurate detection of the transducer shape in real-time during scanning. Another direction is to avoid the need of moving transducer spatially, by using a 2D flexible array. These are the two directions that the research team has been pursuing.

5. Conclusions

In summary, this study has successfully demonstrated the feasibility of using the flexible array ultrasound transducer for the assessment of spinal deformity, using spinal phantoms with different deformity. A comparison was performed among four configurations of the flexible transducer, namely Linear, Convex, Concave and S-shaped, regarding image formation and spinal deformity angle measurements in both coronal and sagittal planes. The results suggested that different configurations had different performances for the image formation on spinous process and the deformity angle measurement. This study paved the way for further investigation about the improvement of the image quality and measurement accuracy under different shapes for the flexible array, mechanism of dynamic shape change during the scanning to fit different body contour, as well as extension from 1D to 2D flexible array.

Author contribution

Conceptualization; Data curation; Formal analysis; Funding acquisition; Investigation; Methodology; Project administration; Resources; Software; Supervision; Validation; Visualization; Roles/Writing - original draft; Writing - review & editing. Elizabeth Ash: Conceptualization, Methodology, Software. Catriona Fennell: Data curation, Writing- Original draft preparation. Linda Gruner: Visualization, Investigation. Ton Bos: Supervision. Ramya Kannan: Software, Validation. Kalaivani Moorthy: Writing- Reviewing and Editing, Supervision. Lucia Muñoz Franco: Data curation, Software, Validation. Queenie Tsung Kwan Shea: Conceptualization, Methodology, Data curation, Formal analysis Writing- Original draft preparation. Yan To Ling: Help on software, idea on the method of comparing 3D coordinate, Writing- Reviewing and Editing. Timothy Tin-Yan Lee: Conceptualize spinous process angle measurement, Sagittal plane deformity analysis, Writing- Reviewing and Editing. Yong Ping Zheng: Conceptualization, Supervision, Funding Acquisition, Writing- Reviewing and Editing.

Funding source

All sources of funding should also be acknowledged and you should declare any involvement of study sponsors in the study design; collection, analysis and interpretation of data; the writing of the manuscript; the decision to submit the manuscript for publication. If the study sponsors had no such involvement, this should be stated. Please state any sources of funding for your research:

Ethical approval and informed consent (if applicable)

If the work involves the use of **human subjects**, the author should ensure that the work described has been carried out in accordance with The Code of Ethics of the World Medical Association (Declaration of Helsinki) for experiments involving humans. The manuscript should be in line with the Recommendations for the Conduct, Reporting, Editing and Publication of Scholarly Work in Medical Journals and aim for the inclusion of representative human populations (sex, age and ethnicity) as per those recommendations. The terms sex and gender should be used correctly.

All **animal experiments** should comply with the ARRIVE guidelines and should be carried out in accordance with the U.K. Animals (Scientific Procedures) Act, 1986 and associated guidelines, EU Directive 2010/63/EU for animal experiments, or the National Institutes of Health guide for the care and use of Laboratory animals (NIH Publications No. 8023, revised 1978). The sex of animals must be indicated, and where appropriate, the influence (or association) of sex on the results of the study.

The author should also clearly indicate in the Material and methods section of the manuscript that applicable guidelines, regulations and laws have been followed and required ethical approval has been obtained.

Patient consent (if applicable)

Completion of this section is mandatory for Case Reports, Clinical Pictures, and Adverse Drug Reactions. Please sign below to confirm that all necessary consents required by applicable law from any relevant patient, research participant, and/or other individual whose information is included in the article have been obtained in writing. The signed consent form(s) should be retained by the corresponding author and NOT sent to Medicine in Novel Technology and Devices.

Declaration of competing interest

The authors declare that there are no conflicts of interest.

Acknowledgements

This work was supported by Hong Kong Research Grant Council (152220/14E, R5017-18), Hong Kong PhD Fellowship Scheme, and the Hong Kong Polytechnic University.

References

[1] Perennou D, Marcelli C, Herisson C, Simon L. Adult lumbar scoliosis. Epidemiologic aspects in a low-back pain population. Spine (Phila Pa 1976;1994(19):123–8. https://doi.org/10.1097/00007632-199401001-00001.

[2] Upadhyay S, Mullaji A, Luk K, Leong J. Relation of spinal and thoracic cage deformities and their flexibilities with altered pulmonary functions in adolescent idiopathic scoliosis. Spine (Phila Pa 1976;1995(20):2415–20. https://doi.org/10.1097/00007632-199511001-00008.

[3] Ascani E, Bartolozzi P, Logroscino C. Natural history of untreated idiopathic scoliosis after skeletal maturity. Spine (Phila Pa 1976;1986(11):784–9. https://doi.org/10.1097/00007632-198610000-00007.

[4] Weinstein SL, Dolan LA, Cheng JCY, Danielsson A, Morcuende JA. Adolescent idiopathic scoliosis. Lancet 2008;371:1527–37. https://doi.org/10.1016/S0140-6736(08)60658-3.

[5] Dickman D, Caspi O. Assessment of scoliosis with Ortelius 800 preliminary results. Clin Appl Notes 2001.

[6] Simony A, Jesper E, Steen H, Christensen B, Carreon LY. Incidence of cancer in adolescent idiopathic scoliosis patients treated 25 years previously 2016;25:3366–70. https://doi.org/10.1007/s00586-016-4747-2.

[7] Cheung CWJ, Zhou GQ, Law SY, Mak TM, Lai KL, Zheng YP. Ultrasound volume projection imaging for assessment of scoliosis. IEEE Trans Med Imag 2015;34:1760–8. https://doi.org/10.1109/TMI.2015.2390233.

[8] Zheng Y, Lee TT, Lai KK, Yip BH, Zhou G, Jiang W, et al. A reliability and validity study for Scolioscan : a radiation-free scoliosis assessment system using 3D ultrasound imaging. Scoliosis Spinal Disord 2016;11:1–15. https://doi.org/10.1186/s13013-016-0074-y.

[9] Wang Q, Li M, Lou EHM, Wong MS. Reliability and validity study of clinical ultrasound imaging on lateral curvature of Adolescent Idiopathic Scoliosis. PloS One 2015;10:135264. https://doi.org/10.1371/journal.pone.0135264.

[10] Ungi T, King F, Kempston M, Keri Z, Lasso A, Mousavi P, et al. Spinal curvature measurement by tracked ultrasound snapshots. Ultrasound Med Biol 2014;40:447–54. https://doi.org/10.1016/j.ultrasmedbio.2013.09.021.

[11] Zheng R, Hill D, Hedden D, Moreau M, Southon S, Lou E. Assessment of curve progression on children with idiopathic scoliosis using ultrasound imaging method. Eur Spine J 2018;27:2114–9. https://doi.org/10.1007/s00586-017-5457-0.

[12] Purnama KE, Wilkinson MHF, Veldhuizen AG. A framework for human spine imaging using a freehand 3D ultrasound system. Technol Health Care 2010;18:1–17. https://doi.org/10.3233/THC-2010-0565.

[13] Brink RC, Wijdicks SPJ, Tromp IN, Schlösser TPC, Kruyt MC, Beek FJA, et al. A reliability and validity study for different coronal angles using ultrasound imaging in adolescent idiopathic scoliosis. Spine J 2018;18:979–85. https://doi.org/10.1016/j.spinee.2017.10.012.

[14] Wong Y-S, Lai KK-L, Zheng Y-P, Wong LL-N, Ng BK-W, Hung AL-H, et al. Is radiation-free ultrasound accurate for quantitative assessment of spinal deformity in idiopathic scoliosis (IS): a detailed analysis with EOS radiography on 952 patients. Ultrasound Med Biol 2019;45:2866–77. https://doi.org/10.1016/j.ultrasmedbio.2019.07.006.

[15] Lee TT-Y, Jiang WW, Cheng CLK, Lai KK-L, To MKT, Castelein RM, et al. A novel method to measure the sagittal curvature in spinal deformities: the reliability and feasibility of 3-D ultrasound imaging. Ultrasound Med Biol 2019;45:2725–35. https://doi.org/10.1016/j.ultrasmedbio.2019.05.031.

[16] Lee TT, Cheung JC-W, To MKT, Cheung JPY, Zheng Y-P. Analysis of sagittal profile of spine using 3D ultrasound imaging: a phantom study and preliminary subject test. Comput Methods Biomech Biomed Eng Imaging Vis 2020;8:232–44. https://doi.org/10.1080/21681163.2019.1566025.

[17] Lou EH, Hill DL, Donauer A, Tilburn M, Hedden D, Moreau M. Results of ultrasound-assisted brace casting for adolescent idiopathic scoliosis. Scoliosis Spinal Disord 2017;12:7–13. https://doi.org/10.1186/s13013-017-0130-2.

[18] Morrison DG, Chan A, Hill D, Parent EC, Lou EHM. Correlation between Cobb angle, spinous process angle (SPA) and apical vertebrae rotation (AVR) on posteroanterior radiographs in adolescent idiopathic scoliosis (AIS) 2015;24:306–12. https://doi.org/10.1007/s00586-014-3684-1.

[19] Delorme S, Labelle H, Aubin CE. De guise JA, Dansereau J. Comparison between clinical Cobb angles and measurements performed on vertebral bodies, pedicle centroids and spinous processes. Ann Chir 1999;53:792–7.

[20] Zhou G, Jiang W, Lai K, Lam T, Cheng CJ, Zheng Y. Semi-automatic measurement of scoliotic angle using a freehand 3-D ultrasound system Scolioscan. IFMBE Proc. 2016;57:341–6. https://doi.org/10.1007/978-3-319-32703-7.

[21] Yu Z, Yu J, Zhang C. Experimental research on PVDF sensing surface characteristic curve applied to topography perception. Micromachines 2020;11. https://doi.org/10.3390/mi11110976.